

Cite this: *J. Mater. Chem. C*, 2019,
7, 13440

A linear D– π –A based hole transport material for high performance rigid and flexible planar organic–inorganic hybrid perovskite solar cells†

Haeun Kwon,[‡] Saripally Sudhaker Reddy,[‡] Veera Murugan Arivunithi,^a Hyunjung Jin,^a Ho-Yeol Park,^a Woosum Cho,^a Myungkwon Song[‡] and Sung-Ho Jin[‡]*

A facile and less expensive hole transport material is essential to enhance the power conversion efficiency (PCE) of perovskite solar cells (PSC) without compromising the ambient stability. Here, we designed and synthesized a new class of HTM by introducing donor– π –acceptor (D– π –A). The HTM was synthesized by combining the moieties of triphenylamine, biphenyl and oxadiazole derivatives as electron donating, π -spacer and electron withdrawing moieties, respectively, named 4'''-(5-(4-(hexyloxy)phenyl)-1,3,4-oxadiazol-2-yl)-N,N-bis(4-methoxyphenyl)-[1,1':4',1'':4'',1'''-quaterphenyl]-4-amine (TPA-BP-OXD). The π – π conjugation is increased by introducing the biphenyl π -spacer. The HTM was terminated with an OXD-based moiety and framed as a D– π –A-based HTM that triggered improvement in the charge transportation properties due to its π – π interactions. We rationally investigated the HTM by characterizing its photophysical, thermal, electrochemical, and charge transport properties. The great features of the HTM stimulated us to explore it on rigid and flexible substrates as a dopant-free HTM in planar inverted-perovskite solar cells (i-PSCs). The device performance in solution processed dopant-free HTM based i-PSC devices on both rigid and flexible substrates showed PCEs of 15.46% and 12.90%, respectively. The hysteresis is negligible, which is one of the most effective results based on a TPA-BP-OXD HTM in planar i-PSCs. The device performance and stability based on the TPA-BP-OXD HTM are better due to higher extraction and transportation of holes from the perovskite material, reduced charge recombination at the interface, and enhanced hydrophobicity of the HTM to compete for a role in enhancing the stability. Overall, our findings demonstrate the potentiality of the TPA-BP-OXD based HTM in planar i-PSCs.

Received 20th July 2019,
Accepted 23rd September 2019

DOI: 10.1039/c9tc03941d

rsc.li/materials-c

Introduction

In the photovoltaics field, organic–inorganic hybrid perovskite solar cells (PSCs) are one of the most effective solar light harvesting technologies, due to their broad absorption spectra, high extinction coefficient, high charge carrier mobility, low exciton binding energy, and excellent semiconducting properties.^{1–7} The excellent features of perovskites have improved the power conversion efficiency (PCE) of PSCs, and it has skyrocketed to 24.2%⁸ by improving the quality of the perovskite layer and reducing recombination by placing suitable interfacial layers *via*

device architectures.⁹ In spite of the high PCE in mesoporous PSCs, the processing temperature for mesoporous based PSCs (> 500 °C) is high for structural modification of mesoporous TiO₂, which restricts their processing with flexible substrates.^{10–12} PSCs of planar-type devices are classified into two types: ETL/perovskite/HTL as regular and HTL/perovskite/ETL as inverted-type PSCs (i-PSCs).^{13–24} Among them, i-PSCs have emerged as a promising tactic to solve the complications accompanying the device structures mentioned above. The simplistic fabrication process of these i-PSCs at low temperature and with low hysteresis evidenced that they are extremely suitable for large scale and flexible PSCs as well.^{10,25–31} Additionally, for commercial application of flexible and rigid i-PSCs, interfacial engineering is required for improvement of the PCE and long term stability.³² Particularly, a HTM is essential for PSCs, which should decrease the recombination rate and realize high efficiency by facilitating a high hole transportation ability. Till now, PSCs based on rigid and flexible substrates widely utilized commercially available state-of-the-art HTMs such as PEDOT:PSS or spiro-OMeTAD. Apart

^a Department of Chemistry Education, Graduate Department of Chemical Materials, Institute for Plastic Information and Energy Materials, Pusan National University, Busandaehakro 63-2, Busan 46241, Republic of Korea. E-mail: shjin@pusan.ac.kr

^b Materials Center for Energy Convergence, Surface Technology Division, Korea Institute of Materials Science (KIMS), 797 Changwondaero, Sungsan-Gu, Changwon, Gyeongnam 642-831, Republic of Korea. E-mail: smk1017@kims.re.kr

† Electronic supplementary information (ESI) available. See DOI: 10.1039/c9tc03941d

‡ These authors contributed equally to this work.

from their advantages, the high hygroscopic nature of PEDOT:PSS, and lower mobility and conductivity, acidic nature, and synthesis complexity of spiro-OMeTAD restrict the further development of PSCs and stability issues have been noticed as key limitations.^{33–35} To overcome these limitations accompanying spiro-OMeTAD and PEDOT:PSS, researchers attempt with inorganic HTMs such as NiO_x, CuSCN, Cu₂O, and V₂O₅ to replace spiro-OMeTAD and PEDOT:PSS.¹⁰ On the other hand, various conjugated polymers have been incorporated in PSCs as HTMs and have shown higher PCEs than PEDOT:PSS and spiro-OMeTAD.^{36–38} Despite the high PCE of inorganic HTMs, they require a high temperature for post-annealing, and thus hinder the fabrication of flexible i-PSCs.

Therefore, organic HTMs are also recommended for high performance rigid and flexible i-PSCs.^{19,39–41} Specifically, organic small molecule (SM) HTMs are used as an efficient candidate for rigid and flexible PSCs. Recently, through rational design and synthesis, we have successfully demonstrated the potentiality of SM HTMs and their multi-applications in PSCs and OSCs.^{32,39} From the above observations, organic SM HTMs are the most promising candidates and the importance of their design is highlighted to maximize high performance and stability for both OSCs and PSCs.

Since triaryl amines have been paid enormous attention in optoelectronic applications due to their hole transporting ability, and chemical and morphological stability,^{32,35,39,41} we have chosen one as one of the key fragments, and further extended with a biphenyl core as a spacer, which increases the π - π interactions and stability of the material,⁴² and eventually terminated the HTM with an oxadiazole (OXD) fragment. OXD is not only known for its good electron accepting property with high PL but also for high thermal and hydrolytic stability and resistance to oxidative degradation.⁴³ The main aim of this linear design is to enhance π - π interactions with enhanced stability. With all aspects herein, we design and report a novel donor- π -acceptor (D- π -A) HTM, 4'''-(5-(4-(hexyloxy)phenyl)-1,3,4-oxadiazol-2-yl)-N,N-bis(4-methoxyphenyl)-[1,1':4',1'':4'',1'''-quaterphenyl]-4-amine (TPA-BP-OXD), by introducing biphenyl as a π -spacer, and it extended the molecular structure, which enhances the π - π conjugation. Finally, the framed D- π -A-based HTM helps to improve the charge transportation properties due to its π - π interactions. It possesses suitable highest occupied molecular orbital (HOMO) energy, high mobility, good solubility, and thermal stability. The dopant-free TPA-BP-OXD-based device exhibited significantly improved device performance in solution-processed i-PSCs with PCEs of 15.46% on rigid and 12.90% on flexible substrates. Negligible hysteresis is observed for the rigid and flexible PSC devices. Additionally, the devices exhibited long term stability over 400 h with minimal loss of the initial performance for both rigid and flexible PSCs.

Results and discussion

Fig. 1 and Fig. S1 (ESI[†]) show the systematic synthesis of the TPA-BP-OXD, D- π -A based HTM. The detailed synthetic procedures are given in the experimental section. Initially, the Suzuki coupling reaction is used to synthesize compound **1**. Compound

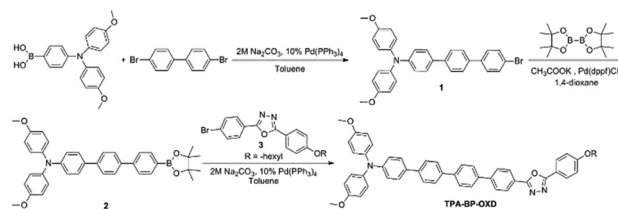


Fig. 1 Synthetic route of HTM TPA-BP-OXD.

1 was further mixed with B₂pin₂, CH₃COOK and Pd(dppf)Cl₂, which resulted in a yield of 63% of compound **2**. The reaction conditions were followed according to our previous reports.⁴⁴ Subsequently compound **3** was synthesized as shown in Fig. S1 (ESI[†]). Last, by coupling of compound **2** and compound **3** under Suzuki conditions, TPA-BP-OXD was synthesized. To confirm TPA-BP-OXD, the material was characterized by ¹H NMR, ¹³C NMR, and HR-MS, and the corresponding detailed synthetic procedures and spectra are provided in the ESI.[†]

The structure of TPA-BP-OXD is shown in Fig. 2(a). The compound consists of TPA as an excellent electron donating moiety, and due to its excellent features, it has been extensively utilized in organic optoelectronic applications. By introducing biphenyl as a π -spacer, it extends the molecular structure, which enhances the π - π conjugation. Finally, the HTM was terminated with an OXD-based moiety and framed as a D- π -A-based HTM that helps to improve the charge transportation properties due to its π - π interactions.

UV-vis absorption spectra of TPA-BP-OXD in CHCl₃ solution and the film state are shown in Fig. 2(b). From the onset absorption spectrum, the optical energy gap (E_g^{opt}) was measured to be 2.67 eV. From Fig. 2(b), the higher energy absorption peak appearing at 317 nm was attributed to the n- π^* transition of triphenylamine, while the low energy band around 358 nm was attributed to intra-molecular charge transfer (ICT). The improved ICT in the film state could be ascribed to the efficient π - π stacking of the HTM in the film state. Furthermore, the temperature dependent and concentration dependent absorption spectra in chlorobenzene solution reveal the existence of ICT as illustrated in Fig. S2 and S3 (ESI[†]), respectively. Even though a similar tendency was observed in the film and solution absorption spectra, there was a shift towards longer wavelength in the absorption spectrum. The absorption peak at higher energy is almost the same as that of the solution, whereas the lower energy peak was shifted toward longer wavelength in the film state, which appeared around 380 nm. This is ascribed to intra-molecular charge transfer between the TPA and the OXD moiety. The maximum emission of TPA-BP-OXD in solution was at 511 nm (Fig. S4, ESI[†]). Thermogravimetric analysis (TGA) and differential scanning calorimetry (DSC) were performed to explore the thermal stability of TPA-BP-OXD. From Fig. 2(c) and (d), TPA-BP-OXD displayed high T_d (corresponding to 5% weight loss) and T_g of 411 °C and 72 °C, respectively. The high thermal stability of HTM is attributed to its linearity.

The electrochemical properties of TPA-BP-OXD were examined using cyclic voltammetry (CV) analysis. Fig. 2(e) shows an

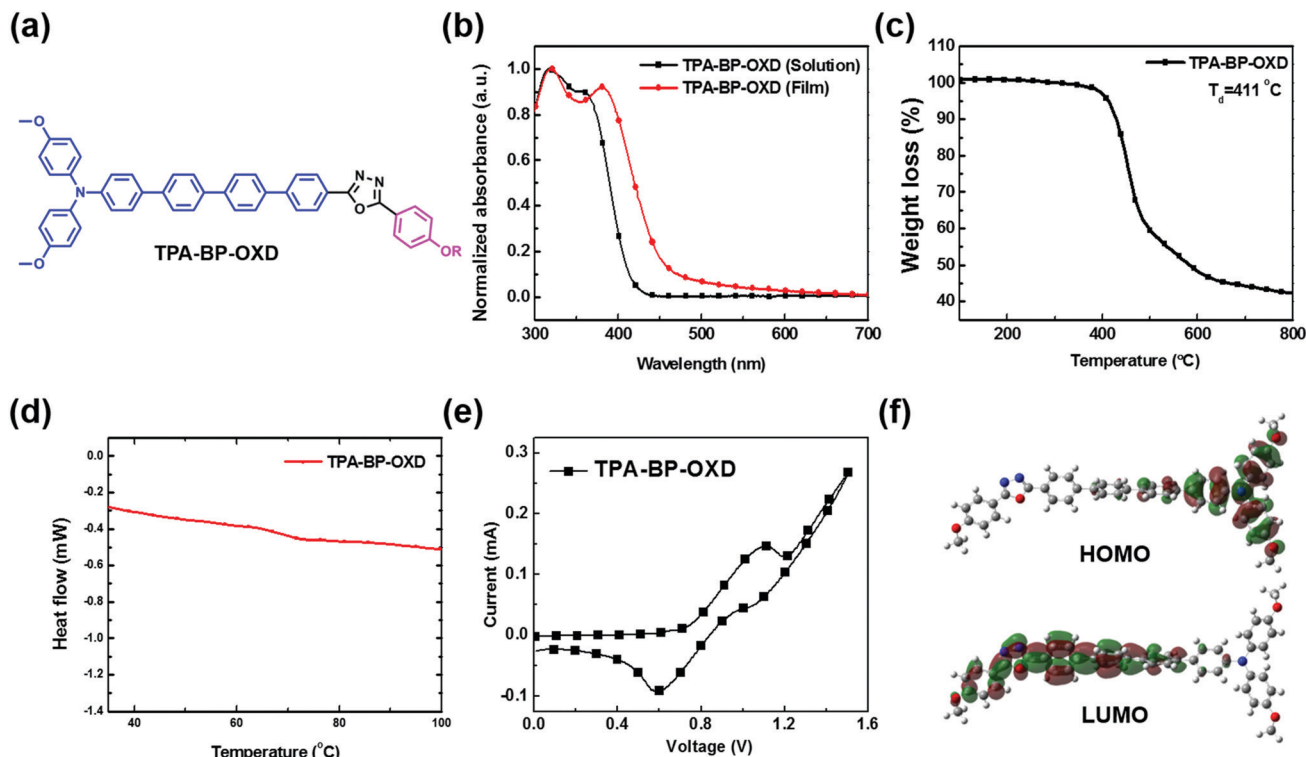


Fig. 2 (a) Molecular structure of the HTM TPA-BP-OXD, (b) UV-vis absorption spectra in solution and the film state, (c) TGA thermogram, (d) DSC trace recorded at a heating rate of $10\text{ }^{\circ}\text{C min}^{-1}$, (e) cyclic voltammogram of TPA-BP-OXD in CH_2Cl_2 solution, and (f) calculated frontier molecular orbitals: calculated spatial distributions of the HOMO and LUMO of TPA-BP-OXD.

irreversible oxidation process of TPA-BP-OXD around 1.2 V in methylene chloride (CH_2Cl_2) solution, which was due to the oxidation of TPA. From CV, the HOMO energy of TPA-BP-OXD was found to be -5.10 eV . The lowest unoccupied molecular orbital (LUMO) energy was calculated from the HOMO energy and $E_{\text{g}}^{\text{opt}}$. From this result, the obtained LUMO value was -2.43 eV . TPA-BP-OXD's obtained HOMO is well matched to the perovskite material valence band, which is beneficial for efficient charge transfer at the interface.

Density functional theory (DFT) has been used to explore and gain further understanding of the geometrical and electronic distribution of TPA-BP-OXD. The electron density of the HOMO was localized on TPA, whereas the LUMO was distributed on the OXD moiety as shown in Fig. 2(f). The calculated HOMO and LUMO of PA-BP-OXD were -4.64 and -1.64 eV , respectively. $E_{\text{g}}^{\text{opt}}$ from DFT was found to be 3.0 eV . The dipole moment was found to be 5.43 D . Furthermore, the dihedral angles are shown in Fig. S5 (ESI[†]). The obtained experimental values and the calculated theoretical values are in good accordance with each other.

The HTM's hole transporting behavior is a major influence on the performance of PSCs. We performed the space-charge-limited current (SCLC) method to elucidate the charge transport potentiality of TPA-BP-OXD with a configuration of ITO/PEDOT:PSS/TPA-BP-OXD/ MoO_3 /Ag as displayed in Fig. S6 (ESI[†]). The hole mobility obtained of TPA-BP-OXD was $3.12 \times 10^{-5}\text{ cm}^2\text{ V}^{-1}\text{ s}^{-1}$.

The device configuration of the rigid and flexible substrates is ITO/TPA-BP-OXD/perovskite/ PC_{61}BM /ZnO NP/Ag, and PET/ITO/TPA-BP-OXD/perovskite/ PC_{61}BM /ZnO NP/Ag, respectively, to explore the potential of the HTM in i-PSCs. The device architecture and energy level diagrams are presented in Fig. 3(a) and 4(a) and (b) respectively. The short-circuit current density–voltage (J - V) characterization of the i-PSCs was carried out under AM 1.5G with simulated solar irradiation at an intensity of 100 mW cm^{-2} . To explore the potentiality of TPA-BP-OXD as a HTM, both rigid and flexible substrate based i-PSCs were fabricated and optimized. The accomplished photovoltaic parameters are summarized in Tables 1 and 2. As shown in Fig. 3(b), the TPA-BP-OXD HTM based i-PSC on a rigid substrate attained an open-circuit voltage (V_{OC}) of 1.03 V , current density (J_{SC}) of 21.15 mA cm^{-2} and fill factor (FF) of 69.59% , and a resulting PCE of 15.19% in the forward scan; in the reverse scan the given PCE was 15.46% with a V_{OC} of 1.03 V , J_{SC} of 21.23 mA cm^{-2} and FF of 70.56% . In addition, the TPA-BP-OXD HTM based device exhibits almost similar J - V curves in the forward and reverse scans.

$$\text{HI} = \frac{\text{PCE}_{\text{Reverse}} - \text{PCE}_{\text{Forward}}}{\text{PCE}_{\text{Reverse}}}$$

From this result, the calculated hysteresis index (HI) was almost negligible for TPA-BP-OXD (0.013) compared with PEDOT:PSS (0.019). A similar trend was observed in the flexible substrate based device as shown in Fig. 4(c). The TPA-BP-OXD HTM based flexible i-PSC shows a V_{OC} of 1.02 V , J_{SC} of 18.81 mA cm^{-2} and FF

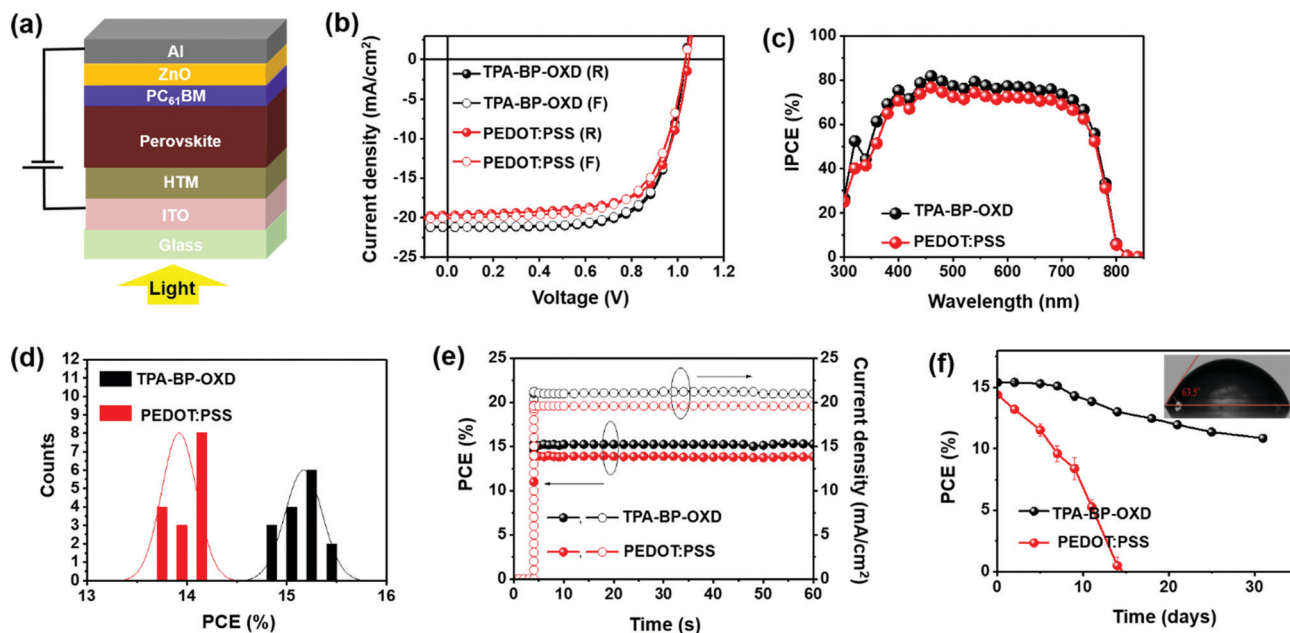


Fig. 3 (a) Rigid device structure of MAPbI₃ based i-PSC, (b) *J*-*V* characteristics, (c) IPCE spectra of rigid i-PSCs with the TPA-BP-OXD HTM, (d) histogram of the rigid i-PSC efficiencies, (e) steady state PCE as a function of time and (f) real PCEs of the i-PSCs as a function of time in days (inset: contact angle of TPA-BP-OXD).

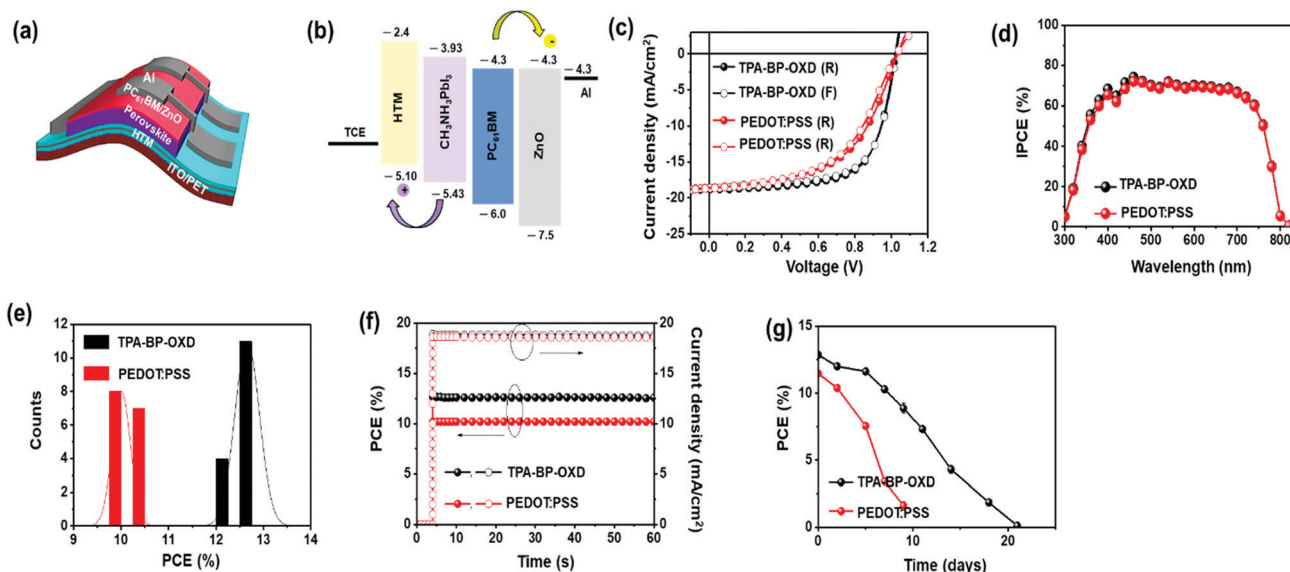


Fig. 4 (a) Flexible device structure, (b) energy level diagram of the MAPbI₃ based i-PSC, (c) *J*-*V* characteristics, (d) IPCE spectra of flexible i-PSCs with TPA-BP-OXD as a HTM, (e) histogram of the flexible i-PSC efficiencies, (f) steady state PCE as a function of time and (g) real PCEs of i-PSCs as a function of time in days.

of 67.14% with a resulting PCE of 12.90% in the forward scan. In the reverse scan direction, the attained PCE was 12.70% with a V_{OC} of 1.02 V, J_{SC} of 18.68 mA cm⁻² and FF of 66.27%. The calculated HI was almost negligible for TPA-BP-OXD (0.015) compared with PEDOT:PSS (0.027). The TPA-BP-OXD based i-PSCs showed superior device performance compared to the PEDOT:PSS based i-PSCs without any additional dopants on the rigid and flexible substrates, due to the slightly enhanced J_{SC} and improved FF. The extracted values of the series resistance (R_s)

and shunt resistance (R_{sh}) from the dark *J*-*V* are summarized in Tables 1 and 2. The standard material using PEDOT:PSS as a HTM was compared with the i-PSCs on the flexible substrate with attributed results of TPA-BP-OXD.

For the confirmation of J_{SC} , the incident photon-to-electron conversion efficiency (IPCE) was measured for the fabricated i-PSCs of TPA-BP-OXD, as shown in Fig. 3(c) and 4(d). The integrated J_{SC} (the forward and reverse scans are 21.28 and 21.39 mA cm⁻², respectively) of the TPA-BP-OXD based devices

Table 1 Photovoltaic performance of rigid i-PSCs with TPA-BP-OXD as dopant-free HTMs

HTM	Scan direction	V_{OC} (V)	J_{SC} (mA cm ⁻²)	FF (%)	PCE (%)	Integrated J_{SC} (mA cm ⁻²)	R_s (Ω cm ²)	R_{sh} (Ω cm ²)
TPA-BP-OXD	Forward	1.03	21.15	69.59	15.19	21.28	2.21	3.06×10^7
TPA-BP-OXD	Reverse	1.03	21.23	70.56	15.46	21.39	2.03	6.30×10^7
PEDOT:PSS	Forward	1.03	20.03	66.56	13.76	20.86	3.29	6.77×10^6
PEDOT:PSS	Reverse	1.04	19.69	68.18	14.04	20.32	3.75	8.90×10^6

Table 2 Photovoltaic performance of flexible i-PSCs with TPA-BP-OXD as dopant-free HTMs

HTM	Scan direction	V_{OC} (V)	J_{SC} (mA cm ⁻²)	FF (%)	PCE (%)	Integrated J_{SC} (mA cm ⁻²)	R_s (Ω cm ²)	R_{sh} (Ω cm ²)
TPA-BP-OXD	Forward	1.02	18.81	67.14	12.90	19.02	4.21	6.23×10^6
TPA-BP-OXD	Reverse	1.02	18.68	66.2	12.70	18.94	4.89	5.10×10^6
PEDOT:PSS	Forward	1.03	18.66	52.09	10.07	18.88	7.31	4.20×10^6
PEDOT:PSS	Reverse	1.03	18.58	53.81	10.35	18.72	7.10	4.62×10^6

calculated from the IPCE spectra values are well matched with the J_{SC} values (the forward and reverse scans are 21.15 and 21.23 mA cm⁻², respectively, for TPA-BP-OXD) resulting from the J - V curves. The same trend is detected in the flexible substrate based i-PSCs. The integrated J_{SC} of TPA-BP-OXD in the flexible i-PSCs was 19.02 and 18.94 mA cm⁻² in the forward and reverse scans, respectively, which are well matched with the J_{SC} values (18.81 and 18.68 mA cm⁻² in the forward and reverse scans, respectively) from the J - V curves. Moreover, the values revealed by the J - V (obtained J_{SC}) and IPCE spectra (integrated J_{SC}) obtained values are in good agreement with a narrow error range. Fig. 3(d) and 4(e) show the histogram of the rigid and flexible substrate PCEs based on both PEDOT:PSS and TPA-BP-OXD. To further confirm the consistency of the J - V measurement, the PCEs of the device were biased at V_{MP} values (voltage at the maximum power point) as a function of time, as shown in Fig. 3(e). The stabilized PCE of the rigid i-PSCs based on PEDOT:PSS and TPA-BP-OXD was linear in time (s) and was found to be 14.04 and 15.46%, respectively, after 60 s. Following a similar technique on flexible substrates for PEDOT:PSS and TPA-BP-OXD, the PCE was found to be 10.35 and 12.70%, respectively, after 60 s (Fig. 4f).

We measured the photoluminescence spectra (PL) and time-resolved PL decay (Fig. S7, ESI[†]) to confirm the extent of the hole extraction behavior of TPA-BP-OXD. The samples were prepared with the configurations ITO/perovskite (MAPbI₃), ITO/PEDOT:PSS/MAPbI₃ and ITO/TPA-BP-OXD/MAPbI₃. Fig. S7(a) (ESI[†]) shows the MAPbI₃ film's high intensity PL spectrum without a HTM, whereas with the introduction of TPA-BP-OXD and PEDOT:PSS (TPA-BP-OXD/MAPbI₃ and PEDOT:PSS/MAPbI₃) the MAPbI₃ absorber intensity was dramatically reduced. In particular, as evidenced by its reduced intensity, TPA-BP-OXD showed efficient PL quenching compared to PEDOT:PSS. Furthermore, for these samples, the transient PL decays were measured as shown in Fig. S7(b) (ESI[†]). τ_1 and τ_2 are denoted as fast and slow decays, respectively. τ_1 and τ_2 of TPA-BP-OXD are 0.83 and 4.68 ns, respectively. Whereas τ_1 and τ_2 of PEDOT:PSS are 1.89 and 5.12 ns, respectively. The average transient decay values achieved were 8.68 ns for ITO/MAPbI₃, 1.89 ns for ITO/PEDOT:PSS/MAPbI₃, and 0.83 ns for ITO/TPA-BP-OXD/MAPbI₃. Compared to PEDOT:PSS and MAPbI₃, the TPA-BP-OXD based film effectively

reduced the decay time, which is beneficial for better extraction of holes from the photogenerated excitons. From the above investigations, we have demonstrated that TPA-BP-OXD was able to extract and transport holes to the electrode efficiently.

A stability test was performed for the fabricated i-PSCs based on TPA-BP-OXD (unencapsulated, temperature: 25 ± 2.5 °C, humidity: $35 \pm 5\%$), as displayed in Fig. 3(f) and 4(g) for rigid and flexible i-PSCs, respectively. The TPA-BP-OXD based i-PSCs with a rigid substrate exhibited high long term stability over 720 h. To know the reason behind the long term stability, a water contact angle (WCA) study was carried out for TPA-BP-OXD. The WCA result for TPA-BP-OXD was 63.5° as shown in Fig. 3f (inset). From the stability study, the TPA-BP-OXD based devices were much more stable than the PEDOT:PSS based i-PCEs. For the rigid i-PSCs, a similar trend has been followed, but the retained PCE is slightly higher than for the flexible devices. The higher hydrophobicity of TPA-BP-OXD is ascribed to the alkoxy tail group found in the HTM design. This phenomenon would restrict the moisture penetration into the perovskite layer, which in turns helps in enhancing the long term stability.³⁹

The surface morphology of the pristine PEDOT:PSS and TPA-BP-OXD and PEDOT:PSS with perovskite and TPA-BP-OXD with perovskite materials was studied using atomic force microscopy (AFM) analyses, as exhibited in Fig. S8 (ESI[†]). The bare HTM film possesses a smooth surface morphology, clearly showing the possibility of efficient charge separation at the HTM/perovskite interface. The bare PEDOT:PSS (root mean square (RMS) = 1.21 nm) and PEDOT:PSS with perovskite (RMS = 8.56 nm) had slightly reduced RMS values when compared to those of the bare TPA-BP-OXD (RMS = 1.42 nm) and TPA-BP-OXD with perovskite (RMS = 11.44 nm) films.

Furthermore, electrochemical impedance spectroscopy (EIS) was performed to gain insight into the interface interactions between PEDOT:PSS/perovskite and TPA-BP-OXD/perovskite based PSCs to depict their hole/charge transport behavior (Fig. S9, ESI[†]). The equivalent circuit model previously reported was used to fit the attained EIS curves.³⁹ R_{rec} decreased in the order TPA-BP-OXD > PEDOT:PSS at low and high voltages, which exhibits a long carrier lifetime for excellent transportation with the i-PSCs of TPA-BP-OXD, and thereby improves the performance of the PSCs. Additionally, the hole conductivity

(σ_{HTM}) was increased with increased voltage due to the higher gradient of the hole density in the HTM. As evidenced by the above investigations, the HTM performance of TPA-BP-OXD was better than that of PEDOT:PSS under the optimized conditions.

Conclusions

In summary, we designed, and well optimized conditions with a simple synthetic approach were used to synthesize, a novel D- π -A based HTM, TPA-BP-OXD. It exhibited a hole mobility of $3.12 \times 10^{-5} \text{ cm}^2 \text{ V}^{-1} \text{ s}^{-1}$, and possessed a suitable energy level (-5.10 eV), good solubility, and high thermal stability (T_d : $411 \text{ }^\circ\text{C}$), which enable it to act as a HTM for PSCs. Notably, the improved charge transportation of TPA-BP-OXD is due to the π - π interactions. The dopant-free TPA-BP-OXD based PSCs exhibited good device performance on rigid ITO (15.46%) and flexible PET substrates (12.90%). Also, they showed long term stability of over 700 h. Efficient extraction of holes from the perovskite and quick transportation to the electrode could be the reason for achieving a higher PCE. The hydrophobic nature of TPA-BP-OXD enhanced the stability of the device. Remarkably, forward and reverse scans of dopant-free TPA-BP-OXD based devices displayed identical performance with negligible hysteresis through excellent compatibility of the linear shaped D- π -A type HTM. Overall, this study demonstrates an efficient linear shaped D- π -A based HTM which can enhance the PCE with less hysteresis, and good stability in i-PSCs on rigid and flexible substrates as well.

Conflicts of interest

There are no conflicts to declare.

Acknowledgements

This work was supported by the National Research Foundation (NRF-2018R1A5A1025594) of the Ministry of Science and ICT. This work was also supported by the Fundamental Research Program (PNK 6100) of the Korea Institute of Materials Science (KIMS).

Notes and references

- 1 A. Kojima, K. Teshima, Y. Shirai and T. Miyasaka, *J. Am. Chem. Soc.*, 2009, **131**, 6050.
- 2 H. Choi, C.-K. Mai, H.-B. Kim, J. Jeong, S. Song, G. C. Bazan, J. Y. Kim and A. J. Heeger, *Nat. Commun.*, 2015, **6**, 7348.
- 3 S. Ameen, M. A. Rub, S. A. Kosa, K. A. Alamry, M. S. Akhtar, H.-S. Shin, H.-K. Seo, A. M. Asiri and M. K. Nazeeruddin, *ChemSusChem*, 2016, **9**, 10.
- 4 S. F. Volker, S. Collavini and J. L. Delgado, *ChemSusChem*, 2015, **8**, 3012.
- 5 W. S. Yang, J. H. Noh, N. J. Jeon, Y. C. Kim, S. Ryu, J. Seo and S. I. Seok, *Science*, 2015, **348**, 1234.
- 6 N. J. Jeon, J. H. Noh, W. S. Yang, Y. C. Kim, S. Ryu, J. Seo and S. I. Seok, *Nature*, 2015, **517**, 476.
- 7 V. M. Arivunithi, S. S. Reddy, V. G. Sree, H.-Y. Park, J. Park, Y.-C. Kang, E.-S. Shin, Y.-Y. Noh, M. Song and S.-H. Jin, *Adv. Energy Mater.*, 2018, **8**, 1801637.
- 8 (a) Q. Jiang, Y. Zhao, X. Zhang, X. Yang, Y. Chen, Z. Chu, Q. Ye, X. Li, Z. Yin and J. You, *Nat. Photonics*, 2019, **13**, 460; (b) Cell efficiency chart, <https://www.nrel.gov/pv/cell-efficiency.html>, accessed: July 2019.
- 9 W. S. Yang, B.-W. Park, E. H. Jung, N. J. Jeon, Y. C. Kim, D. U. Lee, S. S. Shin, J. Seo, E. K. Kim, J. H. Noh and S. I. Seok, *Science*, 2017, **356**, 1376.
- 10 J. Seo, J. H. Noh and S. I. Seok, *Acc. Chem. Res.*, 2016, **49**, 562.
- 11 I. Cho, N. J. Jeon, O. K. Kwon, D. W. Kim, E. H. Jung, J. H. Noh, J. W. Seo, S. I. Seok and S. Park, *Chem. Sci.*, 2017, **8**, 734.
- 12 B. Susrutha, L. Giribabu and S. P. Singh, *Chem. Commun.*, 2015, **51**, 14696.
- 13 M. M. Lee, J. Teuscher, T. Miyasaka, T. N. Murakami and H. J. Snaith, *Science*, 2012, **338**, 643.
- 14 M. Liu, M. B. Johnston and H. J. Snaith, *Nature*, 2013, **501**, 395.
- 15 K. C. Wang, J. Y. Jeng, P. S. Shen, Y. C. Chang, E. W. G. Diau, C. H. Tsai, T. Y. Chao, H. C. Hsu, P. Y. Lin, P. Chen, T.-F. Guao and T.-C. Wen, *Sci. Rep.*, 2014, **4**, 4756.
- 16 Y. J. Jeon, S. Lee, R. Kang, J. E. Kim, J. S. Yeo, S. H. Lee, S. S. Kim, J. M. Yun and D. Y. Kim, *Sci. Rep.*, 2014, **4**, 6953.
- 17 H. Zhou, Q. Chen, G. Li, S. Luo, T.-B. Song, H.-S. Duan, Z. Hong, J. You, Y. Liu and Y. Yang, *Science*, 2014, **345**, 542.
- 18 N. Ahn, D.-Y. Son, I.-H. Jang, S. M. Kang, M. Choi and N.-G. Park, *J. Am. Chem. Soc.*, 2015, **137**, 8696.
- 19 L. Meng, J. You, T.-F. Guo and Y. Yang, *Acc. Chem. Res.*, 2016, **49**, 155.
- 20 M. Saliba, S. Orlandi, T. Matsui, S. Aghazada, M. Cavazzini, J.-P. Correa-Baena, P. Gao, R. Scopelliti, E. Mosconi, K.-H. Dahmen, F. D. Angelis, A. Abate, A. Hagfeldt, G. Pozzi, M. Graetzel and M. K. Nazeeruddin, *Nat. Energy*, 2016, **1**, 15017.
- 21 T. Malinauskas, M. Saliba, T. Matsui, M. Daskeviciene, S. Urnikaite, P. Gratia, R. Send, H. Wonneberger, I. Bruder, M. Grätzel, V. Getautis and M. K. Nazeeruddin, *Energy Environ. Sci.*, 2016, **9**, 1681.
- 22 J. Zhang, B. Xu, M. B. Johansson, M. Hadadian, J. P. C. Baena, P. Liu, Y. Hua, N. Vlachopoulos, E. M. J. Johansson, G. Boschloo, L. Sun and A. Hagfeldt, *Adv. Energy Mater.*, 2016, **1502536**.
- 23 Z. H. Bakr, Q. Wali, A. Fakharuddin, L. S. Mende, T. M. Brown and R. Jose, *Nano Energy*, 2017, **34**, 271.
- 24 (a) Z.-K. Wang, M. Li, Y.-G. Yang, Y. Hu, H. Ma, X.-Y. Gao and L.-S. Liao, *Adv. Mater.*, 2016, **28**, 6695; (b) R. Iacobellis, S. Masi, A. Rizzo, R. Grisorio, M. Ambrico, S. Colella, P. F. Ambrico, G. P. Suranna, A. Listorti and L. D. Marco, *ACS Appl. Energy Mater.*, 2018, **1**, 1069.
- 25 T. Liu, K. Chen, Q. Hu, R. Zhu and Q. Gong, *Adv. Energy Mater.*, 2016, **6**, 1600457.
- 26 Y. Wang, S. Bai, L. Cheng, N. Wang, J. Wang, F. Gao and W. Huang, *Adv. Mater.*, 2016, **28**, 4532.
- 27 F. D. Giacomo, A. Fakharuddin, R. Jose and T. M. Brown, *Energy Environ. Sci.*, 2016, **9**, 3007.

- 28 J. H. Heo, H. J. Han, D. Kim, T. K. Ahn and S. H. Im, *Energy Environ. Sci.*, 2015, **8**, 1602.
- 29 Y. Li, L. Meng, Y. M. Yang, G. Xu, Z. Hong, Q. Chen, J. You, G. Li, Y. Yang and Y. Li, *Nat. Commun.*, 2016, **7**, 10214.
- 30 H. Zhang, J. Cheng, F. Lin, H. He, J. Mao, K. S. Wong, A. K.-Y. Jen and W. C. H. Choy, *ACS Nano*, 2016, **10**, 1503.
- 31 (a) J. Yun, *Adv. Funct. Mater.*, 2017, 1606641; (b) J. H. Heo, D. H. Shin, M. L. Lee, M. G. Kang and S. H. Im, *ACS Appl. Mater. Interfaces*, 2018, **10**, 31413; (c) T. Singh, M. Ikegami and T. Miyasaka, *ACS Appl. Energy Mater.*, 2018, **1**, 6741; (d) G. S. Han, S. Lee, M. L. Duff, F. Qin and J.-K. Lee, *ACS Appl. Mater. Interfaces*, 2018, **10**, 4697.
- 32 S. S. Reddy, S. Shin, U. K. Aryal, R. Nishikubo, A. Saeki, M. Song and S.-H. Jin, *Nano Energy*, 2017, **41**, 10.
- 33 X. Yin, P. Chen, M. Que, Y. Xing, W. Que, C. Niu and J. Shao, *ACS Nano*, 2016, **10**, 3630.
- 34 A. E. Labban, H. Chen, M. Kirkus, J. Barbe, S. D. Gobbo, M. Neophytou, I. McCulloch and J. Eid, *Adv. Energy Mater.*, 2016, **6**, 1502101.
- 35 S. S. Reddy, H. Y. Park, H. Kwon, J. Shin, C. S. Kim, M. Song and S. H. Jin, *Chem. – Eur. J.*, 2018, **24**, 6426.
- 36 K. Kranthiraja, K. Gunasekar, H. Kim, A.-N. Cho, N.-G. Park, S. Kim, B. J. Kim, R. Nishikubo, A. Saeki, M. Song and S.-H. Jin, *Adv. Mater.*, 2017, **29**, 1700183.
- 37 K. Kranthiraja, S. H. Park, H. Kim, K. Gunasekar, G. Han, B. J. Kim, C. S. Kim, S. Kim, H. Lee, R. Nishikubo, A. Saeki, S.-H. Jin and M. Song, *ACS Appl. Mater. Interfaces*, 2017, **9**, 36053.
- 38 K. Kranthiraja, V. M. Arivunithi, U. K. Aryal, H. Y. Park, W. Cho, J. Kim, S. S. Reddy, H.-K. Kim, I.-N. Kang, M. Song and S. H. Jin, *Org. Electron.*, 2019, **72**, 18.
- 39 S. S. Reddy, K. Gunasekar, J. H. Heo, S. H. Im, C. S. Kim, D.-H. Kim, J. H. Moon, J. Y. Lee, M. Song and S.-H. Jin, *Adv. Mater.*, 2016, **28**, 686.
- 40 W. Yan, S. Ye, Y. Li, W. Sun, H. Rao, Z. Liu, Z. Bian and C. Huang, *Adv. Energy Mater.*, 2016, **6**, 1600474.
- 41 S. S. Reddy, V. M. Arivunithi, V. G. Sree, H. Kwon, J. Park, Y. C. Kang, H. Zhu, Y. Y. Noh and S.-H. Jin, *Nano Energy*, 2019, **56**, 284.
- 42 A. Krishna and A. C. Grimsdale, *J. Mater. Chem. A*, 2017, **5**, 16446.
- 43 (a) J. Bettenhausen, M. Greczmiel, M. Jandke and P. Strohmriegel, *Synth. Met.*, 1997, **91**, 223–228; (b) J. A. Mikroyannidis, I. K. Spiliopoulos, T. S. Kasimis, A. P. Kulkarni and S. A. Jenekhe, *Macromolecules*, 2003, **36**, 9295–9302; (c) C. Wang, G. Y. Jung, Y. Hua, C. Pearson, M. R. Bryce, M. C. Petty, A. S. Batsanov, A. E. Goeta and J. A. K. Howard, *Chem. Mater.*, 2001, **13**, 1167–1173.
- 44 (a) S. S. Reddy, V. G. Sree, K. Gunasekar, W. Cho, Y.-S. Gal, M. Song, J.-W. Kang and S.-H. Jin, *Adv. Opt. Mater.*, 2016, **4**, 1236; (b) S. S. Reddy, W. Cho, V. G. Sree and S.-H. Jin, *Dyes Pigm.*, 2016, **134**, 315.